LANGMUIR

pubs.acs.org/Langmuir Article

Interactions of Surfactants with the Bacterial Cell Wall and Inner Membrane: Revealing the Link between Aggregation and Antimicrobial Activity

Pradyumn Sharma,[⊥] Rakesh Vaiwala,[⊥] Srividhya Parthasarathi, Nivedita Patil, Anant Verma, Morris Waskar, Janhavi S. Raut, Jaydeep Kumar Basu,* and K. Ganapathy Ayappa*

Cite This: *Langmuir* 2022, 38, 15714−15728 Read Online

ACCESS | Metrics & More | Article Recommendations | Supporting Information

ABSTRACT: Surfactants with their intrinsic ability to solubilize lipid membranes are widely used as antibacterial agents, and their interactions with the bacterial cell envelope are complicated by their differential aggregation tendencies. We present a combined experimental and molecular dynamics investigation to unravel the molecular basis for the superior antimicrobial activity and faster kill kinetics of shorter-chain fatty acid surfactant, laurate, when compared with the longer-chain surfactants studied in contact time assays with live *Escherichia coli* (*E. coli*). From all-atom molecular dynamics simulations, translocation events across peptidoglycan were the highest for laurate followed by sodium dodecyl sulfate, myristate, palmitate, oleate, and stearate. The translocation kinetics were positively correlated with the critical micellar concentration, which determined the free monomer surfactant concentration available for translocation across peptidoglycan. Interestingly, aggregates showed a lower propensity to translocate across the peptidoglycan layer and longer translocation times were observed for oleate, thereby revealing an intrinsic sieving property of the bacterial cell wall. Molecular dynamics simulations with surfactant-incorporated bacterial inner membranes revealed the greatest hydrophobic mismatch and membrane thinning in the presence of laurate when compared with the other surfactants. The enhanced antimicrobial efficacy of laurate over oleate was further verified by experiments with giant unilamellar vesicles, and electroporation molecular dynamics simulations revealed greater inner membrane poration tendency in the presence of laurate when compared with the longer-chain surfactants. Our study provides molecular insights into surfactant translocation across peptidoglycan and chain length-induced structural disruption of the inner membrane, which correlate with contact time kill efficacies observed as a function of chain length with *E. coli*. The insights gained from our study uncover unexplored barrier properties of the bacterial cell envelope to rationalize the development of antimicrobial formulations and therapeutics.

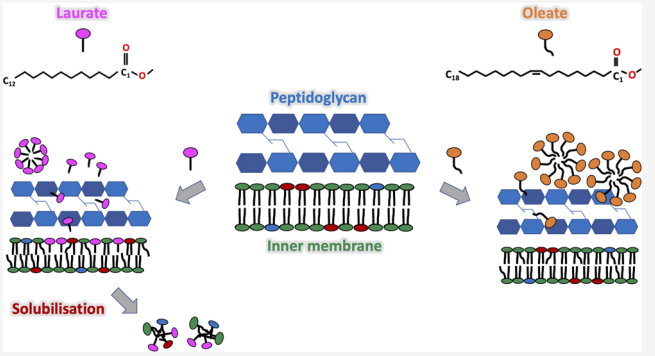

INTRODUCTION

Surfactants and fatty acids with their ability to solubilize lipid membranes are one of the earliest known antimicrobials used widely due to their broad-spectrum activity against bacteria, viruses, and fungi.[1,2] Biosurfactants are also emerging as alternatives to synthetic surfactants due to their low toxicity and biodegradability.[3] Since the common building blocks of both microbial and mammalian cell membranes[4] are phospholipids, surfactants can lyse a wide class of cellular systems. Given the complexity of the bacterial cell envelope and the differences between Gram-negative and Gram-positive cell architectures, a molecular understanding of surfactant interactions with the bacterial cell envelope is needed to improve selectivity and to augment the efficacy of antibacterial action. Additionally, understanding the inhibitory mechanisms of surfactants at molecular scales is vital for adequately assessing the scope and extent of various formulations used as disinfectants and delivering maximum hygiene benefits.

The cell envelope of Gram-negative bacteria (Figure 1) has an outer membrane (OM) made up of lipopolysaccharides and lipids, an intervening periplasmic peptidoglycan layer, and a phospholipid inner membrane,[5] while Gram-positive bacteria are characterized by a thick peptidoglycan layer and an inner membrane. Surfactants and other antimicrobials first bind to the OM of the bacterial cell envelope and penetrate the

Received: September 21, 2022
Revised: November 15, 2022
Published: December 6, 2022

https://doi.org/10.1021/acs.langmuir.2c02520
Langmuir 2022, 38, 15714−15728

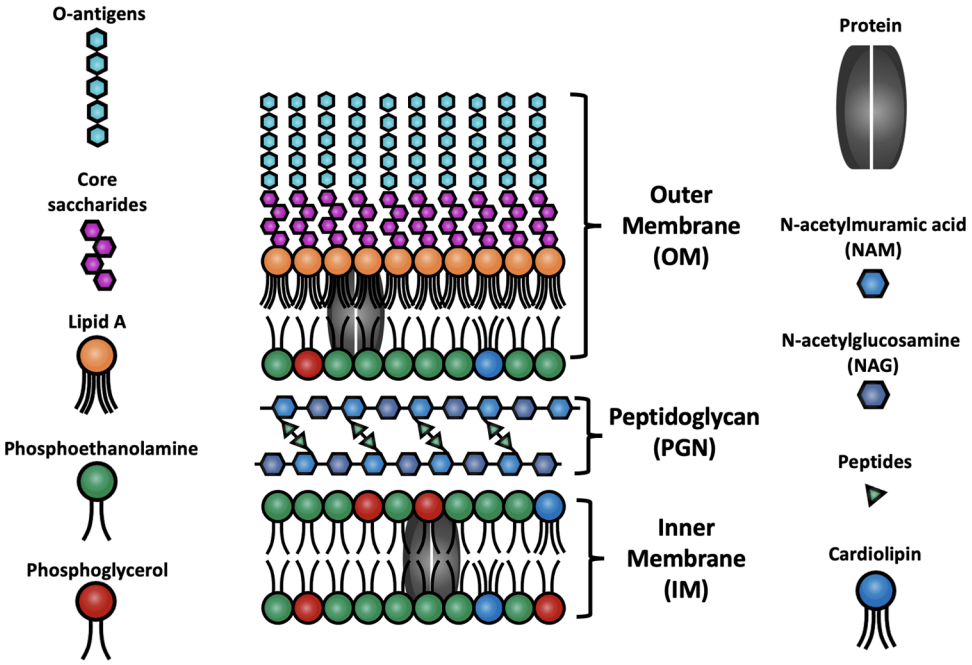

Figure 1. Schematic illustrations of the various molecular components and the cell envelope of Gram-negative *Escherichia coli* bacteria.

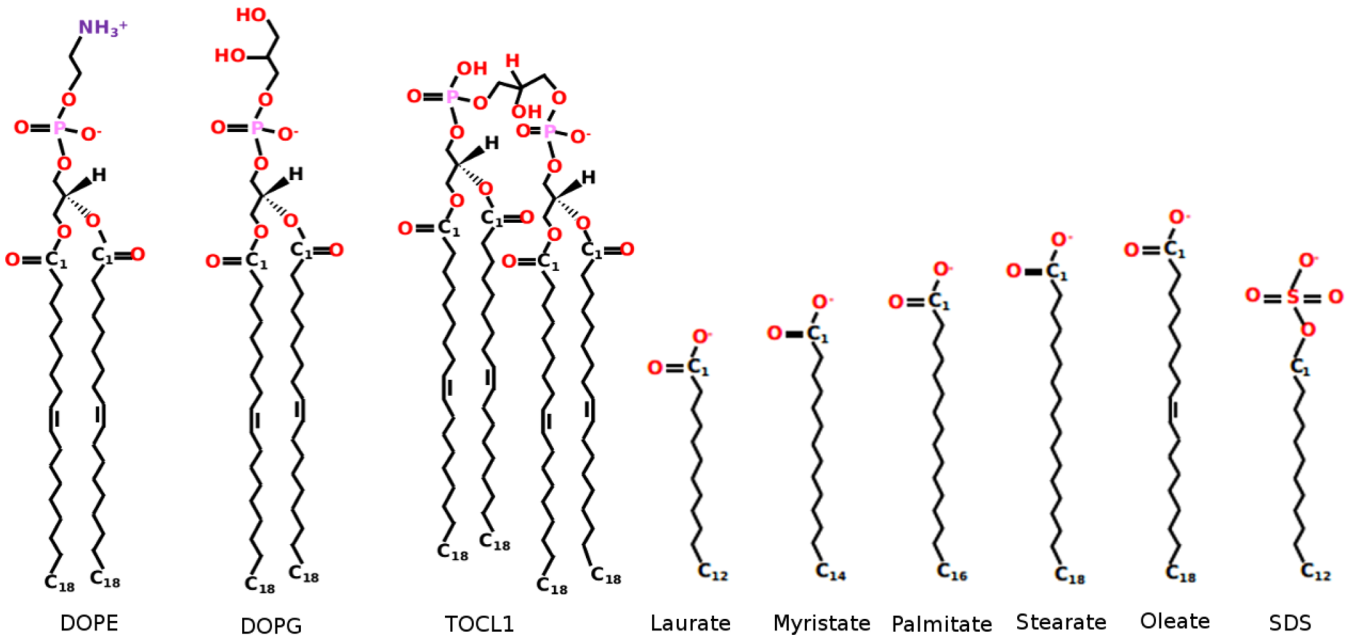

Figure 2. Molecular structures for the lipids, 1,2-dioleoyl-*sn*-glycero-3-phosphoethanolamine (DOPE), 1,2-dioleoyl-*sn*-glycero-3-phospho-rac-1-glycerol (DOPG), and 1,3-bis(1,2-dioleoyl-*sn*-glycero-3-phospho)-glycerol (TOCL1) that constitute the bacterial inner membrane and surfactants laurate, myristate, palmitate, stearate, oleate, and sodium dodecyl sulfate (SDS) used in this study.

bacterial cell wall prior to interacting and solubilizing the phospholipid inner membrane. Due to the negatively charged cell surfaces of both Gram-negative and Gram-positive bacteria, cationic surfactants have been widely used as antibacterial cleansing agents. In particular, quaternary ammonium surfactants[1,6] have been extensively investigated for surface cleansing purposes and fatty acids[7−9] and their derivatives are used primarily in soap formulations. The binding efficacy of the surfactant is a function of several factors, which include size, charge, molecular architecture, and collective properties such as the critical micellar concentration and aggregation numbers,[10] which differ based on their protonation states,[11,12] chain length, and extent of saturation. For nonionic surfactants like disaccharide monoesters, the carbon chain length has been perceived to be the most crucial factor influencing their antimicrobial activity.[13] *N*-Acyl surfactants show variation in antibacterial properties based on chain length and degree of unsaturation,[14] with the presence of double bonds intensifying the antibacterial activity. Hence, a surfactant-specific mechanism is anticipated for these molecules based on chain length, the extent of saturation, charge, and concentration.

Despite the wide use of surfactants and fatty acids as antimicrobial agents, the molecular interactions of these

https://doi.org/10.1021/acs.langmuir.2c02520
Langmuir 2022, 38, 15714−15728

molecules with various components of the bacterial cell envelope are incompletely understood largely due to the inherent complexity of the cell envelope. Whether surfactants solubilize the OM or penetrate the OM through channels to access the inner membrane are open questions. Recent in vitro studies on model bacterial membrane platforms, coupled with super-resolution microscopy methods, indicate that model membrane constructs can potentially be used to assess the barrier characteristics of bacterial membranes.[15−17] However, these experiments are challenging both from the point of constructing reliable bacterial cell wall mimics and using appropriate microscopic tools to interrogate the membrane in the presence of external agents.[15,18] Additionally, surfactant molecules like laurate and oleate are known to exhibit hemolytic activity and it becomes crucial to understand their molecular interactions to augment their selectivity toward bacterial cells.[19−21]

In recent years, molecular dynamics (MD) simulations have evolved as a powerful tool to study bacterial membranes and assess their interactions and free-energy barriers with small molecules and antibiotics. MD simulations have provided a molecular understanding of the barriers offered by different regions of the complex OM,[15,22,23] highlighting the asymmetric free-energy landscape for molecular translocation,[22] which is quite distinct from the inner membrane.[15] The barrier properties of the peptidoglycan layer have recently been investigated in our laboratory.[24,25] Molecular dynamics simulations of surfactants and fatty acids have been widely used to capture properties like self-assembly and partitioning of surfactants[26,27] and also used for investigating the interactions of surfactants with mammalian membrane models.[28,29] However, owing to the complex architecture of the bacterial cell envelope, MD simulations of interactions with surfactants are yet to be reported. A molecular view of surfactant interactions with the cell envelope and subsequent action is only partially understood. With a growing emphasis on antibacterial formulations derived from naturally occurring sources, the focus in this work is primarily on salts of fatty acids, which are the primary constituents for soaps and detergents.

We focus on the hitherto unexplored interaction and translocation of anionic surfactant molecules with the peptidoglycan layer and study the influence of different surfactants on various structural, mechanical, and electric field-induced rupture propensities of the bacterial inner membrane. MD simulations are used to interpret macroscopic observations in contact time kill assays and vesicle rupture studies. We investigate the antimicrobial properties of salts of laurate, dodecyl sulfate (SDS), myristate, palmitate, stearate, and oleate (Figure 2). We perform atomistic MD simulations to provide a molecular explanation for the increased bacterial kill efficacy of laurate over other surfactants to support the observations in contact time kill experiments with *E. coli* suspension. The novelty of our analysis lies in studying the interaction of surfactants with the peptidoglycan layer in addition to the phospholipid inner membrane. Simulations with different surfactant concentrations allow us to study the influence of aggregation behavior on the passage of surfactant molecules through peptidoglycan and also assess the interactions with peptide and glycan moieties with peptidoglycan. The influence of surfactants on the inner membrane properties such as membrane thickness, in-plane lipid order, hydrophobic mismatch, and mechanical properties such as bending modulus and area stretch modulus in the presence of surfactants was examined. To differentiate between different rupture tendencies, electric field-induced poration simulations are carried out, and combined with rupture data from giant unilamellar vesicles, we attribute the varying efficacies of the different surfactants to differences in chain lengths of these molecules. Our study also shows that once the surfactants partition into the inner membrane, the extent to which they perturb the membrane is a function of the surfactant chain length and concentration.

MATERIALS AND METHODS

Bacteria Kill Assays. Surfactants, namely, sodium salts of oleate, laurate, palmitate, stearate, and sodium dodecyl sulfate (SDS), were procured from Sigma-Aldrich. The test bacteria *E. coli* procured from American Type Culture Collection (ATCC 10536) were grown overnight on tryptic soy agar (TSA) plate (procured from Difco TM) at 37 °C and incubated for 16 hours. The cell density was adjusted at optical density 620 (OD620) using a spectrophotometer to get the final count of 10^8 cfu/mL for *E. coli*. A 1 mL of the bacterial suspension was added to 9 mL of surfactant solutions prepared in saline at different concentrations. In the dose-dependent study, bacterial suspensions were treated with 40, 20, 10, and 5 mM of surfactants for 5 min. In the kill kinetics study, different dilutions of sodium oleate and sodium laurate (80, 40, 20, 10, and 5 mM) were incubated with bacterial suspension for 10, 20, 45, and 90 min. After a contact time with the respective concentrations of sodium oleate and sodium laurate, 1 mL of the sample was withdrawn and added to 9 mL of D/E neutralizing broth purchased from Difco TM. The residual bacteria were enumerated by the serial dilution of sample in saline and plating using tryptic soy agar (TSA). After solidification, these plates were incubated at 37 °C for 24 h. The colonies on the plates were counted, and log reduction is calculated by comparing it with the culture control.

Molecular Dynamics Simulations. All-atom molecular dynamics simulations were performed using GROMACS version 5.1.4.[30] The peptidoglycan model was taken from our previous study[24] where a CHARMM36 compatible forcefield was used.[31] The peptidoglycan simulations were carried out with a total of 30 surfactant molecules placed equally on either side of the membrane. In addition, for laurate and oleate, we carried out simulations with 1 and 10 surfactant molecules. The details of the different simulations (Table S1) and protocols used are given in the Supporting Information (SI). Surfactant-incorporated inner membrane models were obtained from the CHARMM-GUI web server.[32] Inner membrane model was procured from our previous work.[15] The membranes containing the potassium salts of laurate, SDS, myristate, palmitate, stearate, and oleate have been studied at surfactant molar concentrations of 40% (Table S2). The membranes with laurate and oleate were also simulated at 20%. In all of the membranes studied, the lipid compositions for DOPE/DOPG/TOCL (TOCL1) correspond to the inner membrane of *E. coli*, viz. ∼75:20:5. The CHARMM36 forcefield[33] was used for surfactants, lipids and ions, while the modified TIP3P[34] water model was employed to model the aqueous solvent. The potassium ions (K^+) were added to maintain electroneutrality. Simulation details for all of the systems examined are given in the SI.

The electroporation studies were carried out for different membrane systems made up of oleate and laurate for electric field strengths in the range of 0.3−0.8 V/nm. For other surfactants, the field strength used is 0.35 V/nm to compare the onset of poration in the different systems. A constant electric field was applied in the positive z-direction, where z is the axis normal to the membrane plane. For each system, three replicas were simulated to obtain the poration time. The onset of poration is defined as the time at which the first continuous chain of water molecules is formed across the bilayer membrane along the z axis, which subsequently grows into an expanding water channel.[35]

https://doi.org/10.1021/acs.langmuir.2c02520
Langmuir 2022, 38, 15714−15728

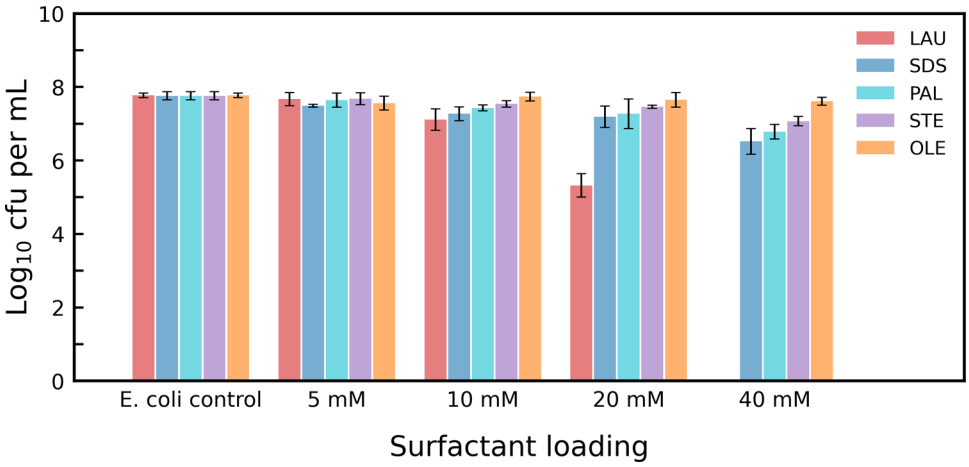

Figure 3. Contact time kill (CTK) data on *E. coli* viability at various concentrations of surfactants for 5 min of exposure. A distinct increase in kill efficacy is observed for sodium laurate when compared with other surfactants.

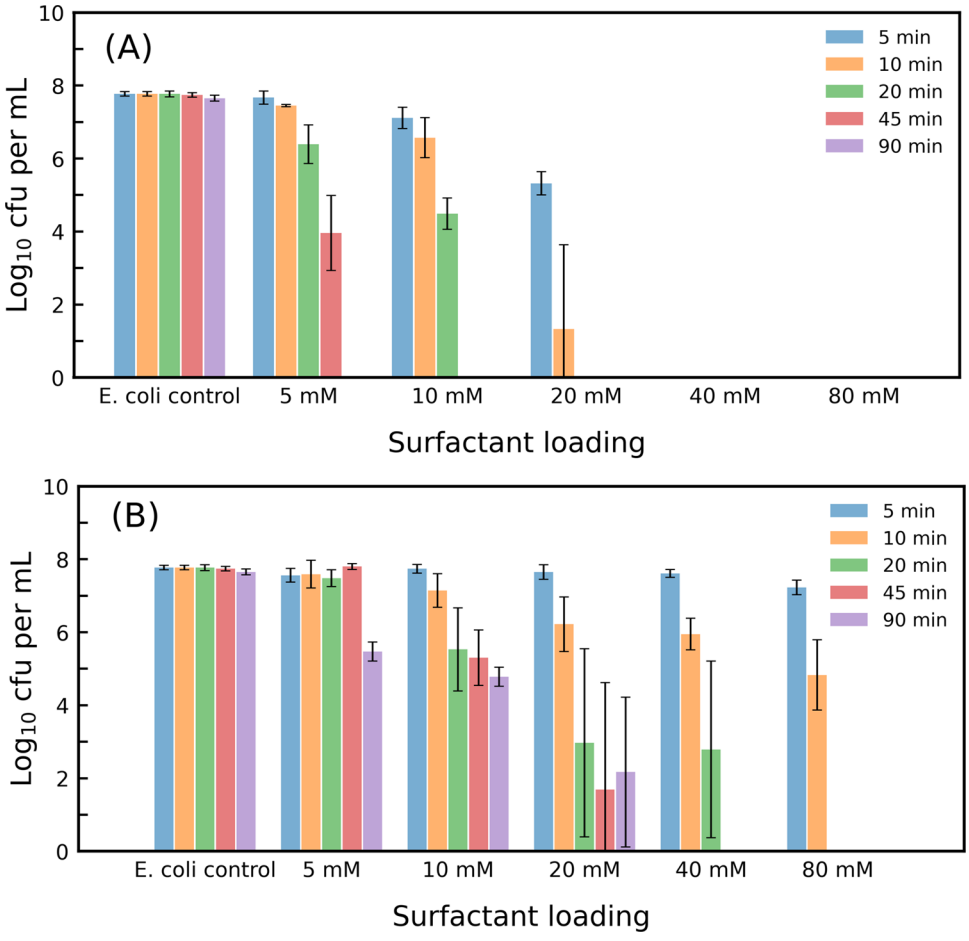

Figure 4. Contact time kill (CTK) data on *E. coli* viability at various concentrations of (A) laurate and (B) oleate. A distinct increase in kill efficacy is observed for sodium laurate when compared with sodium oleate, with enhanced kill efficacy occurring for oleate at longer times.

RESULTS AND DISCUSSION

Efficacy of Short Chain Surfactants. We studied the dose- and time-dependent effect of sodium oleate, laurate, palmitate, stearate, and SDS on *E. coli* viability using contact time kill (CTK) assays (Figure 3) at room temperature (25 °C) and a pH value of 8−8.5. A small decrease in the viable population of bacteria for all surfactants at lower concentrations (<10 mM) is observed at 5 min of exposure time. At a 20 mM concentration, there was a 2 log reduction in *E. coli* viability upon laurate treatment. Other surfactants show reduced efficacy when compared with laurate. Complete kill is observed at 40 mM laurate, and we are able to discern differences in kill efficacy among the other surfactants at 40 mM. SDS showed a 1 log order reduction in bacterial count followed by palmitate, stearate, and oleate, with oleate not showing any efficacy against *E. coli* at a 40 mM concentration.

https://doi.org/10.1021/acs.langmuir.2c02520
Langmuir 2022, 38, 15714−15728

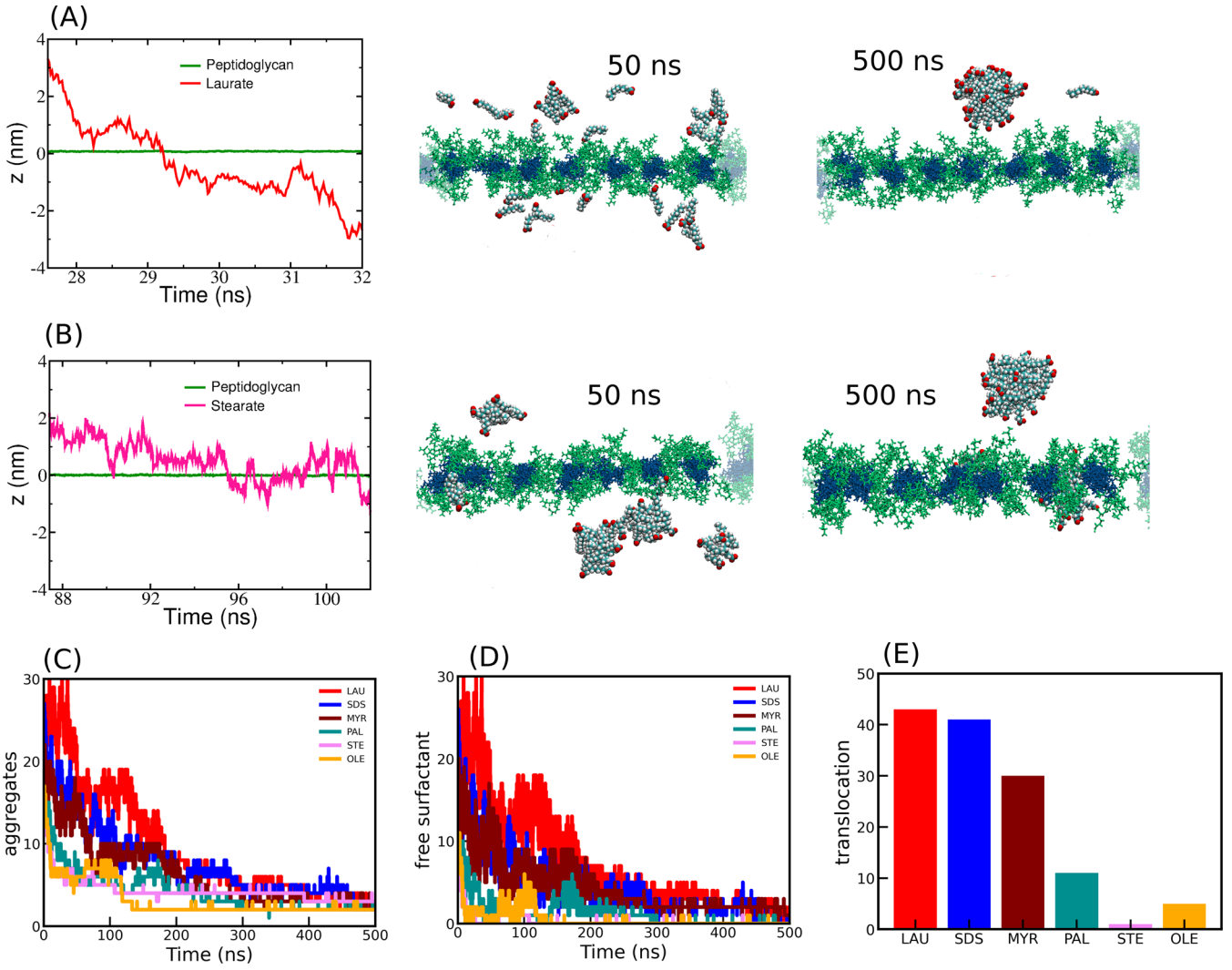

Figure 5. Representative case for the time evolution of the center of mass of *z*-coordinates of the surfactant (laurate in panel (A) and stearate in panel (B)) and the peptidoglycan (green) layer. Also shown are the simulation snapshots at the end of 50 and 500 ns, showing the aggregates of surfactant molecules (laurate in panel (A) and stearate in panel (B)). (C) Time evolution of the number of aggregates and (D) free surfactant over the simulation of 500 ns. (E) The number of translocation events for surfactant molecules during the 500 ns simulation.

These results illustrate that laurate is the most efficacious surfactant against *E. coli* followed by SDS. With the exception of SDS, this is the first signature of the influence of hydrocarbon tail lengths, with a decreasing kill efficacy observed with an increase in carbon atoms. Note that oleate and stearate have the same number of carbon atoms (18); however, stearate is fully saturated.

We also conducted contact time-dependent studies with laurate and oleate for incubation times of bacteria ranging from 5 to 90 min. At the lowest concentration of 5 mM, about a 4 log order reduction is observed at 45 min for laurate (Figure 4A); however, no kill is observed in the case of oleate (Figure 4B). At 90 min, complete kill is observed at the lowest concentration of 5 mM for laurate; however, a similar situation occurs only at 40 mM in the case of oleate. It is observed that at 10 min and 20 min contact times, oleate showed a gradual increase in log reduction with an increase in surfactant dose (Figure 4B). Kill efficacy increased for oleate only at longer times at 45 and 90 min, where it showed a substantial reduction in bacterial counts. The data clearly revealed faster kill kinetics for laurate with complete kill observed above a concentration of 20 mM and a contact time greater than 20 min. In the case of oleate, complete kill occurred only at 80 mM and above a contact time of 20 min. To determine the origins of these differences in activity, we study the interaction of surfactants with peptidoglycan and inner membrane using all-atom MD simulations.

Peptidoglycan: The Unexplored Barrier. We first examined the barrier properties of the peptidoglycan layer to surfactant molecules. The atomistic peptidoglycan model used here[31] yields structural and mechanical properties such as area per disaccharide, thickness (density profile in Figure S1), and area stretch modulus, which are in good agreement with the *E. coli* cell wall.[24] The maximum pore size of peptidoglycan, which might play a crucial role in the barrier characteristics of this membrane, is also comparable with the pore radius reported experimentally.[36,37] We studied the transport of surfactants through peptidoglycan using all-atom molecular dynamics simulations for 30 surfactant molecules. The translocation events were calculated based on the relative positions of the center of mass of peptidoglycan and surfactant molecules, as described in the SI (Figure S2). We observed the

https://doi.org/10.1021/acs.langmuir.2c02520
Langmuir 2022, 38, 15714−15728

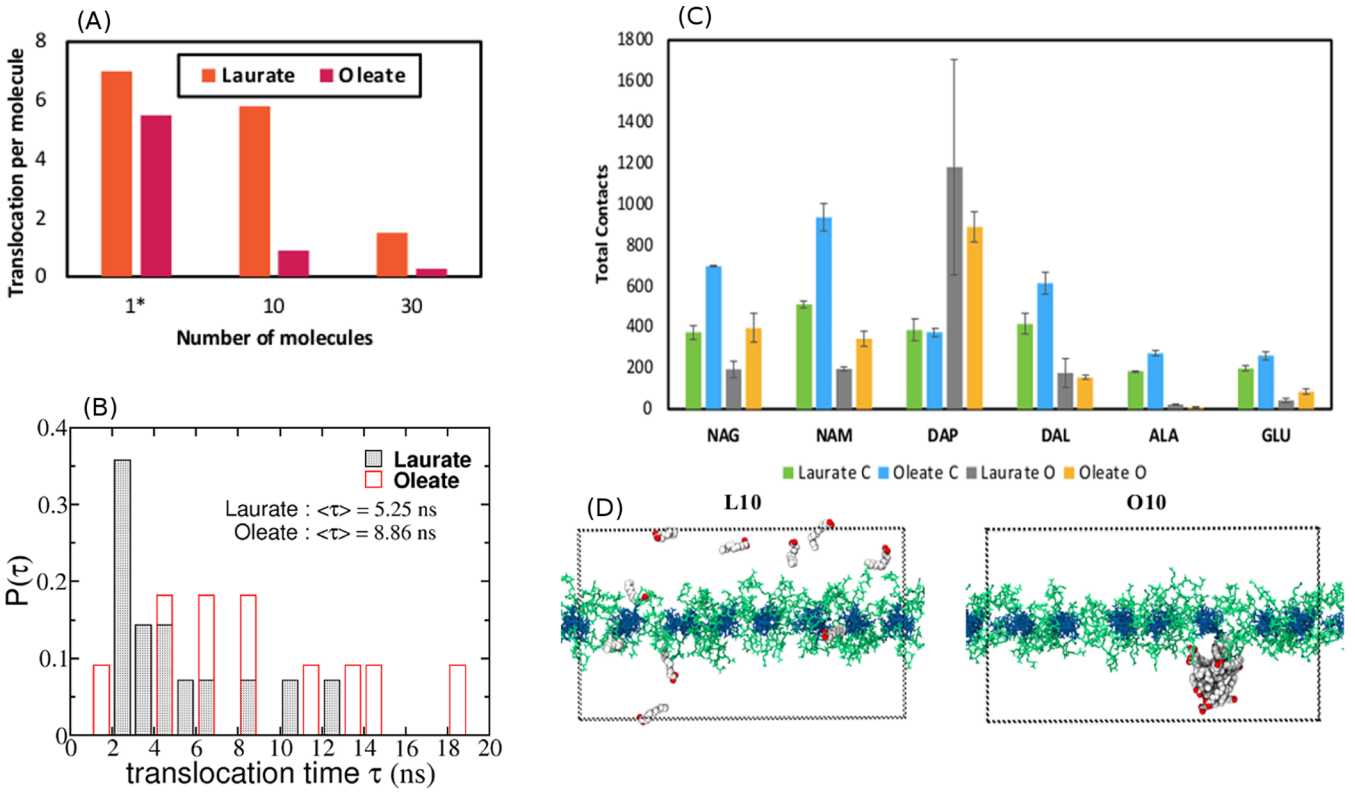

Figure 6. (A) Number of translocation events through peptidoglycan for laurate and oleate molecules. (B) Translocation time distributions for a single laurate and oleate molecule through the peptidoglycan layer. The average translocation time for oleate is higher than that of laurate, indicating the slower rate of translocation for oleate. (C) The total contacts made by carbon and oxygen atoms of surfactants with the peptidoglycan subunits during the course of single surfactant simulations (L1 and O1). (D) Simulation snapshots for systems containing 10 molecules of laurate (L10) and oleate (O10) at the end of 500 ns simulations.

trajectories of an event where a single laurate (Figure 5A) and stearate molecule (Figure 5B) traverse across the peptidoglycan layer. The frequency for such translocation events is a function of the aggregate size since translocation events were observed for aggregates containing both a single surfactant and higher-order aggregates. To further understand the difference in aggregation time scales, we performed a cluster analysis (Figure 5C). In this analysis, a single surfactant molecule is considered a cluster in itself, and once a molecule comes into the vicinity (0.35 nm) of another molecule or aggregate, it becomes part of the corresponding cluster or aggregate. Hence, a decreasing trend in the number of aggregates denotes the formation of larger aggregates during the course of the simulations. Since the concentration with 30 surfactant molecules (37 mM) is above the CMC values of the surfactants, each of the surfactants tends to form micellar aggregates, albeit with different rates (Figure 5C) over the course of the 0.5 μs simulation. The time evolution of the aggregates for the different surfactants (Figure 5C) illustrates that the lifetimes for the smaller aggregates are the largest for laurate followed by SDS, myristate, and palmitate. The longer chain stearate and oleate molecules formed larger aggregates within tens of nanoseconds reflecting the influence of a lower CMC, with both these surfactants having similar aggregation lifetimes. Simulation snapshots at different time points in Figure 5A,B illustrate the increased number of aggregates for stearate and the higher number of free surfactants at earlier times for laurate. The number of free surfactants in aqueous solution are also shown in Figure 5D, where the population of free surfactants follows a similar trend as the aggregate lifetimes. Laurate has the highest survival of monomers, with stearate and oleate having the smallest lifetimes.

We quantify the translocation events across peptidoglycan (Figure 5E) for the different surfactants where we observed that laurate and SDS have a similar number of translocation events followed by myristate, palmitate, oleate, and stearate. The number of translocation events increase in proportion to the survival time of smaller aggregates for each system. Since the kinetics of aggregation is the least for laurate followed by SDS, myristate, palmitate, stearate, and oleate, the number of translocation events are found to be the greatest for laurate when compared with other surfactants (Figure 5E). The translocation events were the lowest for stearate and oleate, with oleate showing a slightly higher number of events compared to stearate. We obtain additional statistics to indicate the size of the aggregate associated with each translocation event (Figure S3). Majority of the translocation events occur for a single surfactant in a monomeric state, with the largest number of events observed for laurate, which has the slowest aggregation kinetics. The greater tendency for other surfactants (having lower CMC values) to aggregate in solution reduces their tendency to translocate (Figure 5C,E). Across the different surfactants, a few translocation events were observed for aggregates containing up to 5 molecules, except in the case of SDS where we observed an 11-molecule aggregate translocating across the membrane. We point out that these events are statistical in nature; however, the time course of 500 ns is sufficient to induce a near-complete aggregation for all the surfactants studied.

https://doi.org/10.1021/acs.langmuir.2c02520
Langmuir 2022, 38, 15714−15728

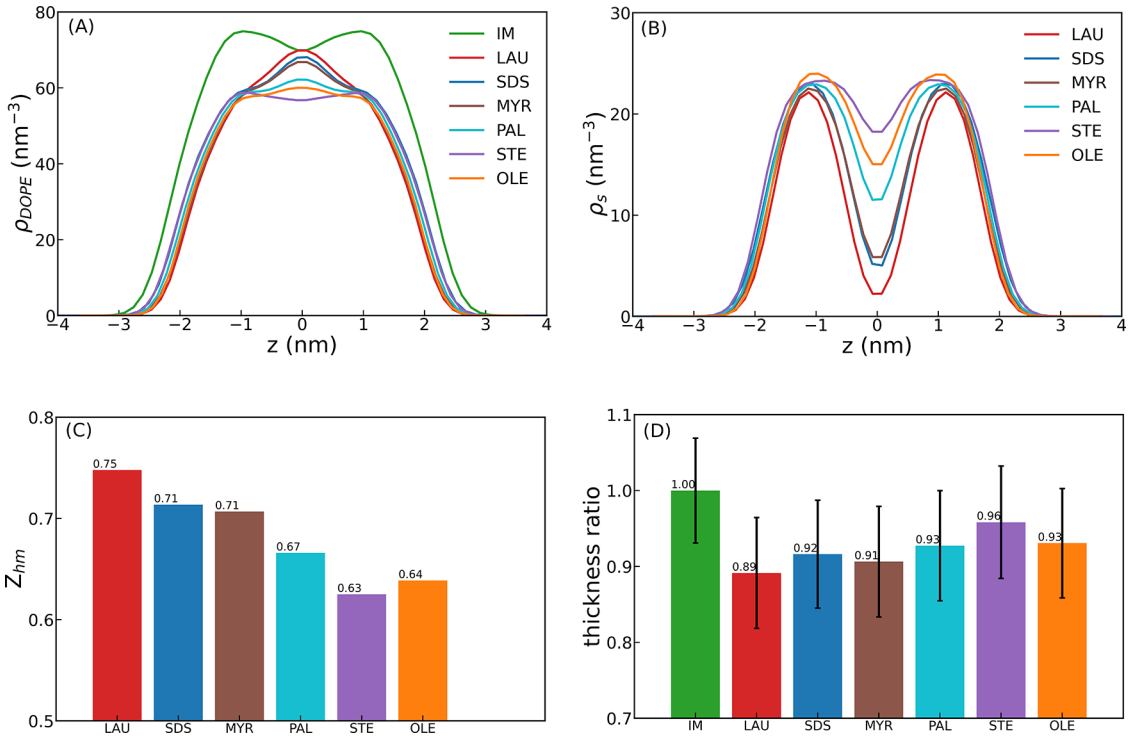

Figure 7. Number density profiles for (A) DOPE lipids, ρ_{DOPE} and for (B) surfactant, ρ_s, along the membrane normal z-direction. (C) Hydrophobic mismatch, Z_{hm}, quantified using eq 1. (D) Membrane thickness scaled by the thickness of the surfactant-free inner membrane (4.081 ± 0.282 nm). IM, inner membrane; LAU, laurate; SDS, sodium dodecyl sulfate; MYR, myristate; PAL, palmitate; STE, stearate; and OLE, oleate.

The trends in aggregation kinetics and the number of translocation events across these surfactants are consistent with their CMC values. Interestingly, the differential trends observed in aggregation kinetics and translocation data across the surfactants are strongly correlated with the CTK data (Figure 3), where laurate showed the highest efficacy in bacterial kill assays and kill efficacy decreased with increasing hydrocarbon chain length. Stearate and oleate were active only at relatively higher concentrations and longer exposure times (Figures 3 and 4B).

Our translocation analysis clearly illustrates the dependence of chain length and related aggregation tendencies that determine the translocation propensity through the peptidoglycan layer. To further elucidate differences between the surfactants, we carried out a detailed study to contrast laurate having the shortest carbon chain (C_{12}) with oleate having the longest carbon chain (C_{18}). Molecular dynamics simulations were carried out with 1 (O1 and L1) and 10 (O10 and L10) molecules for laurate and oleate for 500 ns. Two independent simulations were carried out to improve the statistics for L1 and O1. Multiple translocation events occurred for both L1 and O1 (Figure 6A), providing an explicit confirmation of the lack of any significant barrier in the peptidoglycan layer for a single surfactant molecule. Interestingly, we have also observed differences in the number of translocation events for a single molecule of laurate and oleate (Figure 6A). We observed a total of 14 translocation events for L1 in the two replicas, while for O1, only 11 such events occurred. Representative trajectories of the center of mass of the surfactant illustrate that laurate rapidly crossed the peptidoglycan layer, while oleate resides for longer times in the vicinity of the peptidoglycan layer. We calculated the distribution of passage times (Figure 6B) for translocation events, where the passage time distributions for oleate are broader when compared with laurate, highlighting the variation in translocation kinetics. Furthermore, oleate molecule resides in the vicinity of the peptidoglycan (buffer zone) for almost 42.3% (both replicas) of the simulation trajectory, while for laurate, it was 33.8 and 36.3%. The stronger binding of oleate with the peptidoglycan layer reduces the kinetics of translocation when compared with that of laurate (Figure 6A).

To understand the molecular details of these trends, we have calculated the total contacts (Figure 6C) between the carbon (C) and oxygen (O) atoms of surfactant molecules with the peptidoglycan subunits, namely, *N*-acetylglucosamine (NAG), *N*-acetylmuramic acid (NAM), L-alanine (ALA), D-*iso*-glutamate (GLU), meso-diamino pimelic acid (DAP), and D-alanine (DAL). We have employed a cutoff of 0.4 nm to define these contacts based on the center-of-mass coordinates. The number of contacts for carbon atoms are normalized with respect to the number of carbon atoms in each surfactant molecule. The numbers in Figure 6C represent the average values from two replicates, and the error bars denote the standard error. Surfactant carbon atom contacts are greater when compared with the oxygen headgroups for all peptidoglycan subunits, and with the exception of DAP, the oleate carbon atom contacts are systematically higher when compared with laurate due to the longer residence times of the oleate molecules. The cationic site present in DAP causes a preferential electrostatic attraction for the anionic headgroup of the surfactants. With the exception of DAP, oleate headgroups were found to make a greater number of contacts when compared with the laurate headgroups. In general, the increased number of contacts for oleate correlate positively with the greater residence times for oleate in the vicinity of the peptidoglycan layer resulting in a lower number of translocation events. In summary, this

https://doi.org/10.1021/acs.langmuir.2c02520
Langmuir 2022, 38, 15714−15728

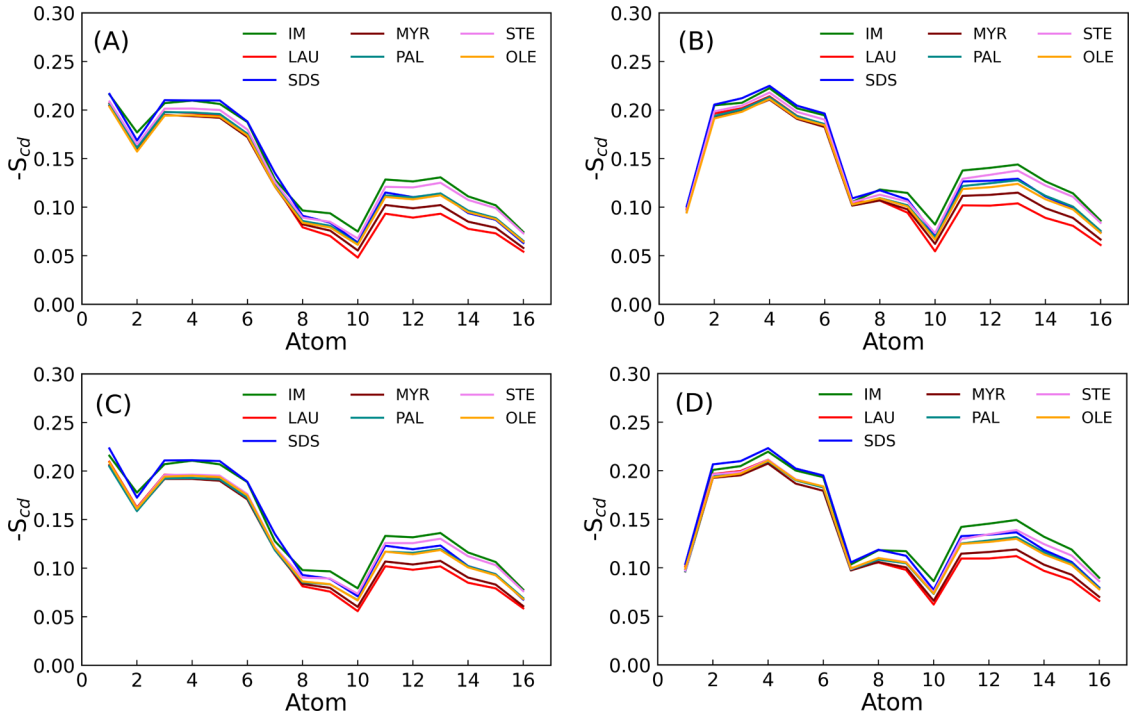

Figure 8. Deuterium order parameters for (A) sn1 chain of DOPE, (B) sn2 chain of DOPE, (C) sn1 chain of DOPG, and (D) sn2 chain of DOPG. IM, inner membrane; LAU, laurate; SDS, sodium dodecyl sulfate; MYR, myristate; PAL, palmitate; STE, stearate; and OLE, oleate.

analysis indicates that the differences in the number of translocation events for the surfactants are determined by the interplay between the interactions of surfactant molecules, with sugars and amino acids present in the peptidoglycan layer.

To observe interactions at intermediate concentrations (11 mM), 500 ns simulations with 10 (L10 and O10) surfactant molecules were carried out (Table S1). Although aggregation was not observed for L10 (Figure 6D), aggregation occurred for the O10 system. The differences in the tendency for aggregate formation can be attributed to the different CMCs for these surfactants, as observed in previous molecular dynamics studies.[27] Potassium oleate[38] having a lower CMC value of 1.2 mM formed a micellar aggregate in the O10 system, while potassium laurate[39] with a higher CMC value of 25 mM did not form the aggregate in L10. Interestingly, these aggregates were unable to translocate through the peptidoglycan layer, resulting in lower translocation events at intermediate as well as higher concentrations.

Surfactant-Induced Thinning in Bacterial Inner Membranes. We next examined the structural and mechanical properties of the surfactant-incorporated Gram-negative inner membrane having 20 and 40% surfactants using 1 μs atomistic simulations (Table S2). Figure S4 illustrates the density distributions for the different lipid components of the bacterial inner membrane incorporated with 40% surfactant. The presence of surfactant induces an overall decrease in the DOPE density upon the addition of surfactant, giving rise to a more uniform density variation within the membrane. The intensity of the well-defined peaks in the vicinity of the headgroups observed for the inner membrane decreases with increasing surfactant concentration, and the overall membrane thickness decreases to accommodate differences in hydrocarbon lengths for the single tail surfactants. Similar trends were observed for the DOPG and TOCL density distributions illustrated in Figures S4 and S5. This provides the first signatures of surfactant-induced disruption of lipid packing within the bilayer.

Figure 7A shows the number density profiles for DOPE lipids for the different surfactant (40%)-incorporated bilayers along the membrane normal. Since the DOPE hydrocarbon tails have 18 carbon atoms, the number density changes in the bilayer midplane reveal variations due to the different tail lengths of the surfactants. The DOPE number density at the bilayer midplane is the highest for laurate followed by SDS, which are both C_{12} surfactants. The number density decreases monotonically for myristate and palmitate followed by stearate. The oleate number density is slightly higher when compared with stearate, reflecting the lowered packing due to the presence of the double bond in the hydrocarbon tail. The surfactant number density (Figure 7B) illustrates a similar trend with chain length, with laurate having the lowest density around the bilayer mid-plane and stearate the highest. Clearly, the different chain lengths of the surfactant cause a density variation inducing bilayer thickness changes when compared to the membrane in the absence of surfactant. We quantify this hydrophobic mismatch Z_{hm} using

$$Z_{hm} = \frac{\int(\rho_{DOPE} - \rho_s)dz}{\int \rho_{DOPE} dz} \quad (1)$$

where ρ_{DOPE} is the number density of DOPE molecules, and ρ_s is the number density of surfactant molecules. We use the DOPE density since this is the dominant lipid component in the bacterial inner membrane. A relatively high degree of hydrophobic mismatch is observed for laurate and the least in the case of stearate (Figure 7C). The membranes containing myristate and SDS show similar mismatch in density, and the larger headgroup of SDS appears to compensate and decrease the mismatch with the longer C_{14} myristate molecules. Z_{hm} monotonically decreases with the chain length of the

https://doi.org/10.1021/acs.langmuir.2c02520
Langmuir 2022, 38, 15714−15728

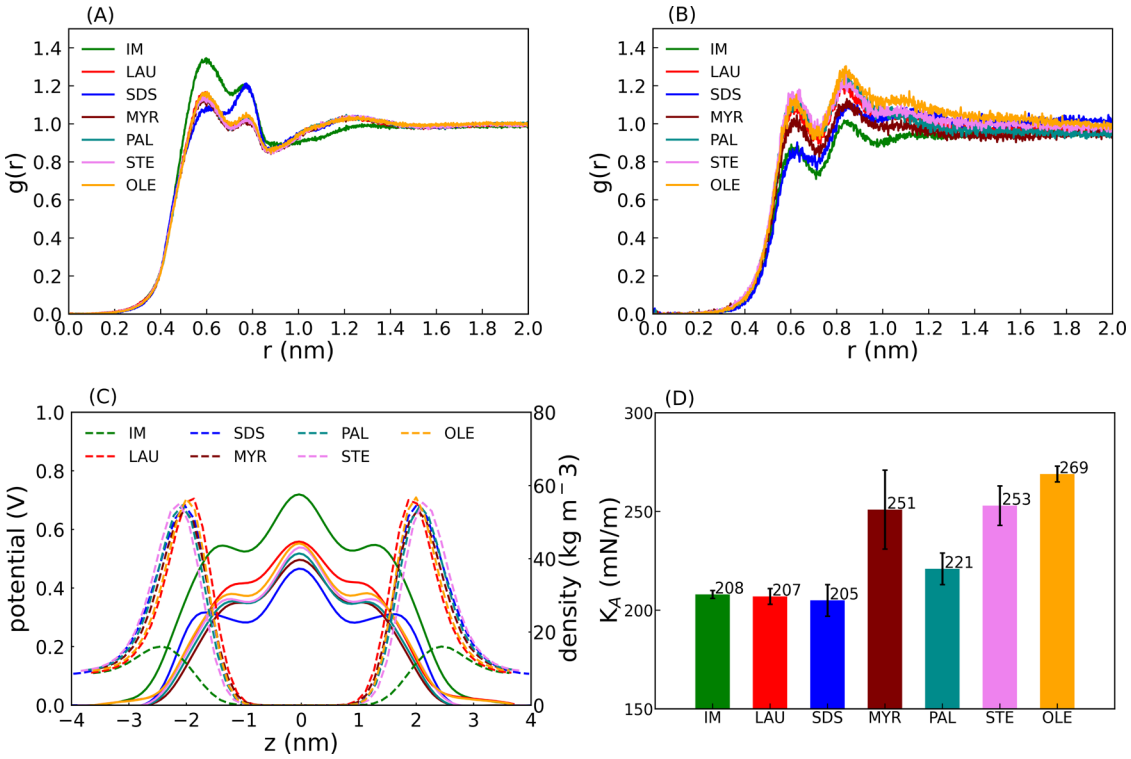

Figure 9. Radial distribution functions $g(r)$ for (A) DOPE−DOPE and (B) DOPG−DOPG. (C) Distributions of electrostatic potential (solid lines) and the density of potassium ions (dashed lines) along membrane normal z. (D) Compressibility modulus for different membrane systems. IM, inner membrane; LAU, laurate; SDS, sodium dodecyl sulfate; MYR, myristate; PAL, palmitate; STE, stearate; and OLE, oleate.

surfactant. The hydrophobic mismatch is best reflected in the membrane thickness, where the thickness is defined relative to the membrane devoid of surfactant (Figure 7D). The membrane thickness is computed using the perl script GridMAT-MD,[40] with the plane of the membrane discretized into 25 × 25 grid points. The phosphorous atoms of lipids, oxygen atoms for carboxyl surfactants, and sulfur atoms of SDS are used to calculate the z-values. The thickness values are averaged over the membrane (grid points) and over time. The membrane thickness is consistent with the trends observed in the hydrophobic mismatch, with the laurate-containing membrane showing the greatest degree of membrane thinning (~90%) decreasing to between 4 and 7% for longer surfactants. The trends observed in the membrane thickness suggest that the shorter laurate molecules having 12 carbon atoms induce a greater extent of hydrophobic mismatch resulting in more significant membrane thinning when compared with the longer stearate and oleate molecules (C_{18} carbon atoms).

The deuterium order parameter for the lipid chains for the different surfactant-mixed membranes is illustrated in Figure 8. The presence of laurate results in a distinct increase in the DOPE tail disorder from C_8 onwards as compared with other surfactant systems. With the exception of SDS, which has a bulky sulfur headgroup, the surfactants show a monotonic trend in order parameter with increasing surfactant chain length; the highest disordering of chains is brought about by laurate, while the least disordering is caused by stearate, which has the same carbon length as that of the membrane lipids. This trend in order parameter with carbon chain length is found to be correlated with the trend in hydrophobic mismatch discussed earlier (Figure 7C). Furthermore, as the concentration of laurate is increased in the membrane, enhanced disordering is observed in lipid chains (Figure S6). However, in the case of oleate, the perturbation to the deuterium order parameter is far less. These structural differences between the laurate and oleate systems indicate that the hydrophobic mismatch induced by the incorporation of the shorter chain laurate molecule results in chain disorder and greater membrane thinning in the bacterial inner membrane. On the contrary, stearate and oleate having 18 carbon atoms are better matched structurally with the uniform 18 carbon atom chains of DOPE, DOPG, and TOCL lipids that make up the inner membrane (Figures 7, S4, and S5).

Electrostatics Play a Role in Lipid−Surfactant Interactions. To elucidate the local structure of the membrane components in the plane of the membrane, we calculated the lipid−lipid radial distribution functions. Since the DOPE content decreases by adding surfactants, the peak heights in the radial distribution functions for the DOPE−DOPE (phosphorous atoms) interactions decrease (Figure 9A). In contrast, the peak heights for DOPG−DOPG interactions increase by adding surfactants (Figure 9B). Differences in the radial distribution functions in the presence of surfactants was minimal, indicating that the different tail lengths do not perturb the correlation or relative packing between the lipid headgroups to a significant extent. However, SDS having a distinctly larger headgroup induces a higher correlation in the radial distribution functions of DOPE−DOPE at the second peak in comparison to other surfactants.

The density of potassium ions in the vicinity of the headgroup atoms increases as the surfactant content is increased (Figure 9C). The net effect of the increased potassium ions in the presence of surfactant results in increased screening of the electrostatic repulsion between the negatively charged headgroups of DOPG resulting in the

https://doi.org/10.1021/acs.langmuir.2c02520
Langmuir 2022, 38, 15714−15728

observed increase in the peak intensities of the pair distribution functions (Figure 9B). The electrostatic potential of the membrane decreases by incorporating anionic surfactants (Figure 9C). The difference is dominant toward the headgroup region attributed to the charged headgroups and increased ion binding, as shown by K^+ ion density (Figure 9C), in the presence of the surfactants. These results indicate that the change in membrane potential is expected to influence the interaction of charged species with the bacterial inner membranes in the presence of surfactants.

Mechanical Properties: Area Stretch Modulus and Bending Modulus. We have calculated the area stretch modulus, K_A, of the membranes using area fluctuations. $K_A = kT\langle A\rangle/\langle(A - \langle A\rangle)^2\rangle$, where A is the instantaneous area of bilayer and $\langle\ \rangle$ denotes a time average. We used block averaging; each block of trajectory was comprised of 10,000 configurations, and the area stretch modulus was calculated for each block. The area stretch modulus for longer-chain surfactants (C_{18}) is relatively higher than that of the membranes containing shorter-chain surfactants, namely, laurate and SDS (Figure 9D). Although we observed a weak decrease in the modulus for the shorter surfactants, laurate and SDS as one would expect, the variations in the standard error do not allow us reliably conclude on the differences between these surfactants. The increase in K_A for the larger hydrocarbon surfactants is consistent with the view that the decreased hydrophobic mismatch results in greater energy to laterally stretch the membrane.

The energy associated with the local curvature of a membrane can be estimated from the bending modulus (κ_c) using the Helfrich formulation,[41] as described in the SI. The bending modulus for the inner membrane (Figure S7) is estimated to be 29.1 kT, which is in good agreement with a value of 28.7 kT reported for a pure DOPE membrane.[42] This comparison is justified since the inner membrane is mainly composed of DOPE lipids. The bending moduli for the membranes studied here reveal that the surfactant-mixed membranes are softer ($\kappa_c \sim 15-21\ kT$) when compared with the membrane devoid of surfactants.

Electroporation Studies. Compromising the integrity of the bacterial membrane involves several mechanisms, which are incompletely understood. However, membrane rupture and solubilization in the presence of surfactants are a likely cause for cell membrane damage and occur on the time scales of seconds or minutes, as observed in the CTK data lying well beyond the time scales accessible in molecular dynamics simulations. To shed light on the differential rupture tendencies in the presence of the surfactants investigated in this work, we resorted to electric field-induced poration simulations, which have been widely used to study poration in phospholipid bilayers.[35,43−46]

Figure S8A illustrates the variation in initial poration times (see the Materials and Methods section) at an applied electric field of 0.35 V/nm for the different inner membranes with a 40% surfactant loading. The increase in membrane area monitored as a function of time for each of the three replicates for laurate and oleate is illustrated in Figure S9 (A,B), and snapshots of the water channel illustrating the onset of pore formation and growth are illustrated in Figure S9 (C,D). With the exception of SDS, the poration times in general were found to decrease with a decrease in the surfactant hydrocarbon chain length. Laurate showed the highest reduction of 1 order when compared with the bare membrane, and SDS had the highest poration time when compared with the other surfactants. Poration is initiated by the reorientation of the lipid and surfactant molecules to form a stable water pore. The poration times reflect this reorientational dynamics, and the presence of surfactants clearly enhances this pore-forming tendency. The high poration time for SDS could be attributed to the bulky sulfate headgroups in comparison with the smaller carboxylic acid headgroups of the other fatty acid-based surfactants. Additionally, the reorientational energy is expected to be lowered for thinner membranes and we qualitatively observe that laurate, which results in the greatest bilayer thinning (Figure 7D), has the smallest poration time (Figure S8). Once the pore has formed, the pore growth rates are likely to be influenced by the mechanical properties such as the area stretch modulus, and we observed an increase in the modulus with increasing surfactant chain length (Figure 9D) consistent with the increased poration times for these systems (Figure S8). From the changes in membrane area with time (Figure S9), growth rates were smaller for oleate when compared with those for laurate. We also studied the influence of membrane composition and obtained electroporation times for the membranes containing 20% oleate and laurate and compared the poration times as a function of voltage for the 40% membranes (Figure S8B). At lower surfactant concentration, the poration times increase and a stronger dependence on the imposed voltage is observed. The voltage dependence is the least for the laurate membranes where poration times are less than 2 ns (for L40) for all of the voltages studied. In contrast, O40 membranes reveal a distinct voltage dependence, consistent with the lowered tendency of oleate to alter membrane properties when compared with that of laurate.

Reconciling CTK Data Trends. We connect the differences observed in the interactions of the different surfactants with the bacterial membranes with contact time kill (CTK) experiments performed on Gram-negative bacteria. We point out that although the experiments were carried out with the sodium salts of fatty acids and the MD simulations were carried out with the corresponding potassium salts, we propose a general guiding principle for the differences in their actions based on the CMC values for the different surfactants. The CTK analysis conferred better efficacy for sodium laurate at higher concentrations (>10 mM) in agreement with previous studies on corresponding protonated fatty acids,[47] as observed by a considerable reduction in the viable population of bacteria. The shorter chain surfactants, laurate and SDS, show better bacterial kill efficacies compared to longer chain surfactants, palmitate, stearate, and oleate. The kill propensity for oleate is weaker, and we did not observe any significant level of antibacterial activity even up to 40 mM surfactant concentration (Figure 3). We propose that these differences between the antimicrobial action of surfactants are driven in part by the higher CMC values ($CMC^L \sim 25$ mM) and the shorter-chain length of sodium laurate (C_{12}) when compared with the lower CMC value, $CMC^O \sim 9$ mM for sodium oleate.[48,49] Since the free surfactant concentration (C_{sf}) is limited by the CMC[50,51] (C_{sf} = CMC), bacteria are exposed to higher monomeric concentrations of the shorter surfactant when compared with the longer surfactants having lower CMC values.

Our molecular dynamics study shows the changes in translocation of the different surfactants across the peptidoglycan layer, with a monotonic decrease in translocation events with increasing surfactant chain length (lower CMC). The

https://doi.org/10.1021/acs.langmuir.2c02520
Langmuir 2022, 38, 15714−15728

peptidoglycan did not pose a barrier for monomers; however, translocation kinetics of a single laurate molecule was faster when compared with that of oleate. We report that these differences are based on the interplay between the interactions of surfactant molecules with sugar and amino acid subunits of the peptidoglycan layer. Peptidoglycan offered a barrier to surfactant aggregates, and higher CMC values resulted in an increased single molecule population[27] when concentrations were above the CMC. Apart from having differences in kill efficacy due to different CMCs, the surfactants also differ in their kinetics of antibacterial activity. Our CTK analysis as a function of time (Figure 4) reveals faster kinetics for laurate when compared with that of oleate. Thus, at concentrations where complete kill occurs for laurate, increased exposure time enhanced the antibacterial activity for oleate (Figure 4).

The availability of free surfactant and hence the translocation events across peptidoglycan decreased monotonically for myristate, palmitate, and stearate as the CMC values decrease with increasing chain length. Larger micellar aggregates are unable to translocate through the peptidoglycan layer, as illustrated in our MD simulations, and activity is dictated by the availability of free surfactant. This explanation is in good agreement with the CTK data where kill efficacy was found to decrease with increasing chain length. For the case of oleate, if the antimicrobial activity sets in above the CMC, the formation of micelles prevents the concentration of free surfactant from exceeding the CMC value. The differences in the barrier offered by peptidoglycan for these molecules at higher concentrations explain the differences in the observed antibacterial activity of these molecules toward *E. coli* (Figure 10). Next, we briefly comment on SDS and oleate. SDS has a distinctly larger headgroup when compared with the other fatty acids, with a similar chain length as laurate (C_{12}). Due to the lower CMC of SDS (8 mM), our simulations show relatively faster aggregation kinetics and lower translocation events for SDS when compared with those for laurate. This trend is reflected in the CTK data as well, where SDS has a lowered kill efficacy compared to laurate (Figure 3). The difference between stearate and oleate is the presence of the double bond for oleate. This difference did not significantly alter the aggregation kinetics, and marginal differences were observed in the CTK data.

In addition to the differences in the mechanism and barriers offered to surfactant molecules by the peptidoglycan layer, the inner membrane interactions also play a crucial role. Our surfactant-incorporated inner membrane atomistic models were found to be stable over the course of the simulation and we did not observe any ripple formation, as observed in previous studies of surfactant/cosurfactant membranes.[52] However, among the key observations, the lipid tails become increasingly disordered, and the bilayers show a reduction in the membrane thickness with increasing surfactant concentration. In general, these changes were greater and more accentuated in the case of the shorter chain laurate molecules when compared with those of other surfactants. We attributed the observed differences between laurate and other surfactants primarily to the increased hydrophobic mismatch for laurate, which is 12-carbon long, while the lipid chains are 18-carbons in length, similar to that of stearate and oleate. The presence of laurate decreases the correlations between DOPE molecules to a greater extent when compared with that of oleate, indicating the greater disorder induced due to the increased hydrophobic mismatch. An opposite effect in the correlations is observed for

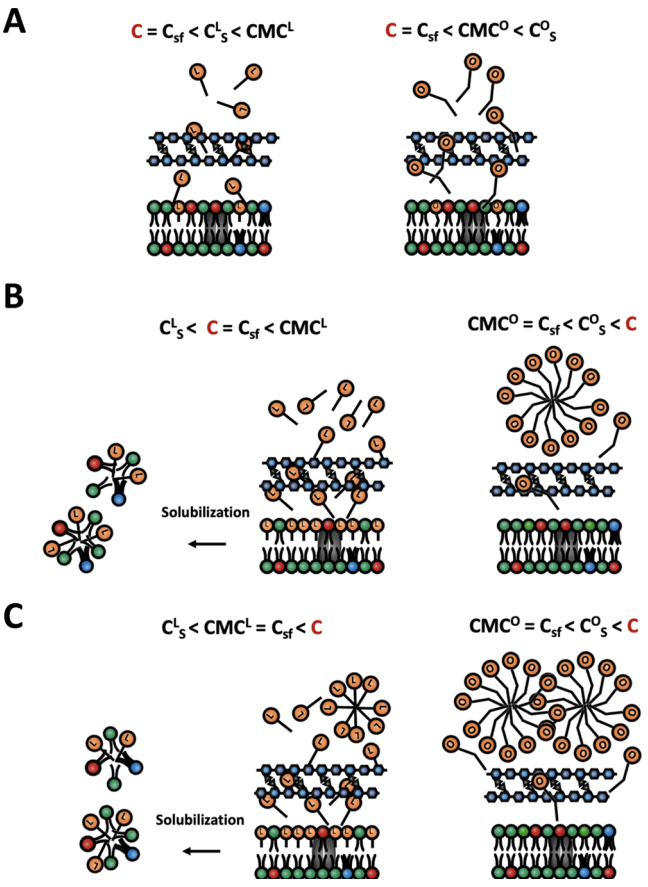

Figure 10. Schematic illustration of the translocation of surfactant molecules across the peptidoglycan layer (blue) and solubilization of the inner bilayer membrane based on surfactant concentrations and CMC values. C and C_{sf} are the total and free surfactant concentrations, respectively. Critical micelle concentrations for laurate and oleate are represented by CMC^L and CMC^O, respectively. Laurate and oleate concentrations required for inner membrane solubilization are represented by C_S^L and C_S^O, respectively. (A) Low surfactant concentration with no killing activity, (B) intermediate concentration where single laurate molecules are active, and (C) both laurate and oleate form micelles; however, only laurate is active due to sufficient single-molecule surfactant concentration.

DOPG molecules, which are smaller in content in the inner membrane. The changes in the charge interactions are attributed to higher ion binding with increasing surfactant concentrations. This decreases the membrane potential and can influence the interaction of charged species like cationic antimicrobial peptides with the inner membrane. This could also explain the reason for the synergistic effects exhibited by the surfactants with cationic peptides.[53] The change in membrane potential can also affect the local organization of proteins involved in cell division.[54] We have shown that the mechanical properties such as bending modulus and the area stretch modulus are modulated by the hydrophobic mismatch induced by surfactants, with a general trend observed wherein the area stretch modulus increased with increasing chain length with a lowering of the bending modulus in surfactant-incorporated membranes.

Vesicle Rupture Experiments. It is widely accepted that surfactants can "solubilize" bacterial membranes; however, the precise molecular mechanisms are unknown. Several mechanisms have been discussed in the literature[4] with reference to

https://doi.org/10.1021/acs.langmuir.2c02520
Langmuir 2022, 38, 15714−15728

the inner membrane, largely drawn from vesicle rupture-based mechanisms. According to a three-stage mechanism[55−57] of vesicle solubilization, the surfactant molecules at low concentration first partition between aqueous solution and the vesicle. The partitioning is characterized by the distribution coefficient. At higher surfactant concentration, the vesicle is saturated with the surfactant, and the concentration of free surfactant molecules in aqueous solution at this saturation point corresponds to the CMC. Finally, further addition of surfactant results in the formation of mixed micelles composed of both lipids and surfactant, resulting in vesicle solubilization. In the above models, it is assumed that the surfactant molecule has access to the inner membrane and its subsequent rupture controls antimicrobial activity. To further examine the action of surfactants and their connection with inner membrane rupture, we performed experiments with Cy5 dye-encapsulated giant unilamellar vesicles (GUVs) composed of *E. coli* total extract whose composition is predominantly that of the bacterial inner membrane. The details for GUV preparation and the key observations on rupturing of the GUVs with surfactants are given in the SI. As shown in Figure S10, oleate caused GUV rupture at higher concentrations (> 12 mM) when compared with laurate (> 9 mM). It can be inferred from these experiments that the minimum surfactant concentration required for inner membrane rupture is lower in the case of laurate (C_S^L = 9 mM) as compared to that of oleate (C_S^O = 12 mM). Note that C_S^L = 9 mM is much lower than the corresponding CMC value of sodium laurate; however, C_S^O = 12 mM is only slightly larger than the CMC for sodium oleate. We point out that with confocal measurements, the highest resolution is ∼244 nm and we are unable to observe changes associated with bilayer thinning, which occur on length scales below 5 nm. Additionally, when rupture occurs, the event is usually catastrophic (Figure S10); however, we were able to observe a more gradual decrease in size for sodium oleate at 12 mM (Figure S10 (B,E)) and the radius of curvature was found to increase exponentially with time. Electroporation molecular dynamics simulations, which provide a close connection with the GUV rupture experiments, illustrate the higher propensity for rupture when laurate is present and show a general increase in rupture times with surfactant chain length. These results provide additional data to support the increased tendency for laurate to induce membrane rupture when compared with the longer chain oleate molecule.

An aspect that is not completely understood is the transport of surfactants to the bacterial inner membrane. In the case of Gram-negative bacteria, surfactants could access the inner membrane through defects created in the outer membrane or through outer membrane transporters. In this regard, FadL transporters[58] are known to allow the transport of fatty acids. However, the possibility of surfactant transport through outer membrane channels is unclear. Since both oleate and laurate molecules are able to pass through the peptidoglycan layer, albeit at different rates, they would be able to access the inner membrane. Solubilization would then follow, provided the concentration of surfactant at the inner membrane is sufficiently high. This hypothesis, which supports the view that surfactant action occurs at the inner membrane, is also corroborated by the good agreement between the C_S^L (9 mM) observed in GUV rupture (Figure S10) and the threshold concentration (10 mM) for observing a 1 log reduction in viable bacterial population in the case of sodium laurate (Figure 3). Thus, the laurate molecule concentration at the inner membrane is sufficiently high to cause solubilization of the inner membrane and kill the bacteria. With regard to oleate, we argue that if oleate molecules access the inner membrane, its concentration is limited by the CMC, which is below the threshold concentration to induce rupture in the inner membrane. This notion is also supported by the higher concentration required by oleate to rupture GUVs. Although the inner membrane is widely implicated in surfactant-mediated membrane solubilization, the interaction of the surfactants with the OM is unclear.

If laurate action is driven by solubilization of the outer membrane, then it is likely that oleate would also follow a similar mode of action. Since the concentration of free surfactant is limited by its CMC,[51] the lower monomeric concentration for oleate could preclude the OM solubilization if this indeed was the primary mechanism of antibacterial action. Additional investigations would have to be carried out to determine the interactions and possible solubilization action of surfactants on the bacterial outer membrane. It is possible that antibacterial activity can be driven by a combination of the outer membrane and inner membrane solubilization, and given the complex architecture of the outer membrane with the increased interaction between long chain lipopolysaccharides, the solubilization kinetics are expected to be slow when compared to that of the inner membrane. In either event, the availability of surfactant to the peptidoglycan and inner membrane would be dependent on the CMC. A final point to note is related to time scales for different processes. Translocation kinetics from the MD simulations are on the order of about 100s of nanoseconds and kill kinetics range from a few minutes to hours depending on the surfactant concentration. We point out that the peptidoglycan is in an ionic solution in our MD simulations. In reality, the periplasm where the peptidoglycan is located is rich in enzymes and proteins that could influence both the availability of surfactant at the peptidoglycan and consequently lower the surfactant flux through this layer. Further, the differential inner membrane binding of surfactants and solubilization time scales for the outer membrane lipopolysaccharides could also determine the bacterial kill kinetics.

We summarize our findings in Figure 10, which provides a schematic illustration of the aforementioned mechanism, which assumes that surfactants are able to access the inner membrane and induce membrane rupture and damage. If the free surfactant concentration, C_{sf}, is below the respective CMC values as well as below the inner membrane solubilization concentrations for laurate (C_S^L) and oleate (C_S^O), kill activity is absent (Figure 10A). Additionally, if C_{sf} is above solubilization concentration and below CMC, then kill activity would occur, as illustrated in Figure 10B. The aforementioned kill mechanism is expected for surfactants like laurate. While in the case of longer surfactants like oleate where $C_S^O > CMC^O$, C_{sf} will not exceed CMC^O, hence limiting its kill activity (Figure 10B,C). Laurate, however, will be effective even above CMC^L, as the C_{sf} is greater than the corresponding C_S^L. These effects will also be modulated by the availability of micellar aggregates whose equilibrium would shift toward monomeric surfactants as the surfactants translocate across the membrane.

CONCLUSIONS

Using a combination of experiments and molecular dynamics simulations, we differentiate between the action of surfactants, whose primary differences lie in the hydrocarbon tail lengths,

https://doi.org/10.1021/acs.langmuir.2c02520
Langmuir 2022, 38, 15714−15728

with both the inner membrane and intervening peptidoglycan layer of Gram-negative bacteria. Our study reveals that the peptidoglycan cell wall, generally perceived to be a passive barrier for transport, serves as a filter modulating the translocation of surfactants based on their physicochemical and aggregation properties, providing insights into an unexplored regime of transport across the bacterial cell wall. We specifically provide insights into the modulation of the inner membrane structural and mechanical properties as a function of surfactant chemistry—in this case, the surfactants of different chain lengths. The critical concentration required for bacterial kill is related to the CMC, which determines the availability of surfactant at the membrane interface. Our study reveals that both the availability of free surfactant and the kinetics of translocation play an important role in the antibacterial activity. Additional investigations would be required to confirm the role of protein channels for surfactant transport as well as the tendency for surfactants to solubilize the OM of Gram-negative bacteria. Our study provides a quantitative framework to assess the antibacterial efficacy of surfactant molecules. The methods and insights presented here can be extended to evaluate interactions of other surface-active molecules and optimize antibacterial formulations.

■ ASSOCIATED CONTENT

Supporting Information

The Supporting Information is available free of charge at https://pubs.acs.org/doi/10.1021/acs.langmuir.2c02520.

Calculations for translocation events, electrostatic potential and bending modulus, GUV preparation, density profiles, deuterium order parameters, and electroporation times, pore growth, and GUV rupture data (PDF)

■ AUTHOR INFORMATION

Corresponding Authors

Jaydeep Kumar Basu − *Department of Physics, Indian Institute of Science, Bangalore 560012, India;* orcid.org/0000-0002-6683-4732; Phone: +91-80-2293 3281; Email: basu@iisc.ac.in

K. Ganapathy Ayappa − *Department of Chemical Engineering, Indian Institute of Science, Bangalore 560012, India;* orcid.org/0000-0001-7599-794X; Phone: +91-80-2293 2769; Email: ayappa@iisc.ac.in

Authors

Pradyumn Sharma − *Department of Chemical Engineering, Indian Institute of Science, Bangalore 560012, India;* Present Address: Eli Lilly Services India Private Limited, Bangalore 560103, India; orcid.org/0000-0002-4489-1832

Rakesh Vaiwala − *Department of Chemical Engineering, Indian Institute of Science, Bangalore 560012, India;* orcid.org/0000-0003-1862-8659

Srividhya Parthasarathi − *Department of Physics, Indian Institute of Science, Bangalore 560012, India*

Nivedita Patil − *Unilever Research and Development, Bangalore 560066, India*

Anant Verma − *Department of Chemical Engineering, Indian Institute of Science, Bangalore 560012, India*

Morris Waskar − *Unilever Research and Development, Bangalore 560066, India*

Janhavi S. Raut − *Unilever Research and Development, Bangalore 560066, India;* orcid.org/0000-0002-0586-1219

Complete contact information is available at: https://pubs.acs.org/10.1021/acs.langmuir.2c02520

Author Contributions

⊥P.S. and R.V. contributed equally to this work.

Notes

The authors declare no competing financial interest.

■ ACKNOWLEDGMENTS

The authors thank Unilever Research and Development (Bangalore, India) for funding this research and Scott Singleton for valuable discussions. The authors also thank the Supercomputer Education and Research Center (SERC) for availing computational facility at the Indian Institute of Science, Bangalore, the Department of Science and Technology, India, and the National Supercomputing Mission (NSM) for funding computational resources used for part of this study. Srividhya Parthasarathi is supported by Kothari Postdoctoral fellowship from UGC, Government of India.

■ REFERENCES

(1) Falk, N. A. Surfactants as Antimicrobials: A Brief Overview of Microbial Interfacial Chemistry and Surfactant Antimicrobial Activity. *J. Surfactants Deterg.* **2019**, *22*, 1119−1127.

(2) Hoefler, B. C.; Gorzelnik, K. V.; Yang, J. Y.; Hendricks, N.; Dorrestein, P. C.; Straight, P. D. Enzymatic resistance to the lipopeptide surfactin as identified through imaging mass spectrometry of bacterial competition. *Proc. Natl. Acad. Sci. U.S.A.* **2012**, *109*, 13082−13087.

(3) Santos, D. K. F.; Rufino, R. D.; Luna, J. M.; Santos, V. A.; Sarubbo, L. A. Biosurfactants: multifunctional biomolecules of the 21st century. *Int. J. Mol. Sci.* **2016**, *17*, 401.

(4) Heerklotz, H. Interactions of surfactants with lipid membranes. *Q. Rev. Biophys.* **2008**, *41*, 205.

(5) Im, W.; Khalid, S. Molecular Simulations of Gram-Negative Bacterial Membranes Come of Age. *Annu. Rev. Phys. Chem.* **2020**, *71*, 171−188.

(6) Zhang, S.; Ding, S.; Yu, J.; Chen, X.; Lei, Q.; Fang, W. Antibacterial activity, in vitro cytotoxicity, and cell cycle arrest of gemini quaternary ammonium surfactants. *Langmuir* **2015**, *31*, 12161−12169.

(7) Yoon, B. K.; Jackman, J. A.; Valle-González, E. R.; Cho, N.-J. Antibacterial free fatty acids and monoglycerides: biological activities, experimental testing, and therapeutic applications. *Int. J. Mol. Sci.* **2018**, *19*, 1114.

(8) Nakatsuji, T.; Kao, M. C.; Fang, J.-Y.; Zouboulis, C. C.; Zhang, L.; Gallo, R. L.; Huang, C.-M. Antimicrobial property of lauric acid against Propionibacterium acnes: its therapeutic potential for inflammatory acne vulgaris. *J. Invest. Dermatol.* **2009**, *129*, 2480−2488.

(9) Huang, C. B.; Alimova, Y.; Myers, T. M.; Ebersole, J. L. Short- and medium-chain fatty acids exhibit antimicrobial activity for oral microorganisms. *Arch. Oral Biol.* **2011**, *56*, 650−654.

(10) Laatiris, A.; el Achouri, M.; Infante, M. R.; Bensouda, Y. Antibacterial activity, structure and CMC relationships of alkanediyl α, ω-bis (dimethylammonium bromide) surfactants. *Microbiol. Res.* **2008**, *163*, 645−650.

(11) Morrow, B. H.; Koenig, P. H.; Shen, J. K. Self-assembly and bilayer-micelle transition of fatty acids studied by replica-exchange constant pH molecular dynamics. *Langmuir* **2013**, *29*, 14823−14830.

(12) Janke, J. J.; Bennett, W. D.; Tieleman, D. P. Oleic acid phase behavior from molecular dynamics simulations. *Langmuir* **2014**, *30*, 10661−10667.

(13) Zhang, X.; Song, F.; Taxipalati, M.; Wei, W.; Feng, F. Comparative study of surface-active properties and antimicrobial activities of disaccharide monoesters. *PLoS One* **2014**, *9*, No. e114845.
(14) Joondan, N.; Jhaumeer-Laulloo, S.; Caumul, P.; Akerman, M. Synthesis, physicochemical, and biological activities of novel N-acyl tyrosine monomeric and Gemini surfactants in single and SDS/CTAB-mixed micellar system. *J. Phys. Org. Chem.* **2017**, *30*, No. e3675.
(15) Sharma, P.; Parthasarathi, S.; Patil, N.; Waskar, M.; Raut, J. S.; Puranik, M.; Ayappa, K. G.; Basu, J. K. Assessing barriers for antimicrobial penetration in complex asymmetric bacterial membranes: A case study with thymol. *Langmuir* **2020**, *36*, 8800−8814.
(16) Michel, J. P.; Wang, Y.; Kiesel, I.; Gerelli, Y.; Rosilio, V. Disruption of asymmetric lipid bilayer models mimicking the outer membrane of Gram-negative bacteria by an active plasticin. *Langmuir* **2017**, *33*, 11028−11039.
(17) Paracini, N.; Clifton, L. A.; Lakey, J. H. Studying the surfaces of bacteria using neutron scattering: finding new openings for antibiotics. *Biochem. Soc. Trans.* **2020**, *48*, 2139−2149.
(18) Sarangi, N. K.; Ilanila, I.; Ayappa, P. K. G.; Visweswariah, S. S.; Basu, J. K. Super-resolution stimulated emission depletion-fluorescence correlation spectroscopy reveals nanoscale membrane reorganization induced by pore-forming proteins. *Langmuir* **2016**, *32*, 9649−9657.
(19) Pinazo, A.; Pons, R.; Marqués, A.; Farfan, M.; da Silva, A.; Perez, L. Biocompatible Catanionic Vesicles from Arginine-Based Surfactants: A New Strategy to Tune the Antimicrobial Activity and Cytotoxicity of Vesicular Systems. *Pharmaceutics* **2020**, *12*, 857.
(20) Mishima, M.; Wakita, Y.; Nakano, M. Studies on the promoting effects of medium chain fatty acid salts on the nasal absorption of insulin in rats. *J. Pharmacobio-Dyn.* **1987**, *10*, 624−631.
(21) Jumaa, M.; Müller, B. W. Lipid emulsions as a novel system to reduce the hemolytic activity of lytic agents: mechanism of the protective effect. *Eur. J. Pharm. Sci.* **2000**, *9*, 285−290.
(22) Carpenter, T. S.; Parkin, J.; Khalid, S. The free energy of small solute permeation through the *Escherichia coli* outer membrane has a distinctly asymmetric profile. *J. Phys. Chem. Lett.* **2016**, *7*, 3446−3451.
(23) Sharma, P.; Ayappa, K. G. A Molecular Dynamics Study of Antimicrobial Peptide Interactions with the Lipopolysaccharides of the Outer Bacterial Membrane. *J. Membr. Biol.* **2022**, *255*, 665−675.
(24) Vaiwala, R.; Sharma, P.; Puranik, M.; Ayappa, K. G. Developing a Coarse-Grained Model for Bacterial Cell Walls: Evaluating Mechanical Properties and Free Energy Barriers. *J. Chem. Theory Comput.* **2020**, *16*, 5369−5384.
(25) Vaiwala, R.; Sharma, P.; Ayappa, K. G.Differentiating interactions of antimicrobials with Gram-negative and Gram-positive bacterial cell walls using molecular dynamics simulations. *Biointerphases* 2022, *17* (6), DOI: 10.1116/6.0002087.
(26) Shinoda, W.; DeVane, R.; Klein, M. L. Coarse-grained molecular modeling of non-ionic surfactant self-assembly. *Soft Matter* **2008**, *4*, 2454−2462.
(27) King, D. T.; Warren, D. B.; Pouton, C. W.; Chalmers, D. K. Using molecular dynamics to study liquid phase behavior: simulations of the ternary sodium laurate/sodium oleate/water system. *Langmuir* **2011**, *27*, 11381−11393.
(28) Bandyopadhyay, S.; Shelley, J. C.; Klein, M. L. Molecular dynamics study of the effect of surfactant on a biomembrane. *J. Phys. Chem. B* **2001**, *105*, 5979−5986.
(29) Pizzirusso, A.; de Nicola, A.; Sevink, G. A.; Correa, A.; Cascella, M.; Kawakatsu, T.; Rocco, M.; Zhao, Y.; Celino, M.; Milano, G. Biomembrane solubilization mechanism by Triton X-100: a computational study of the three stage model. *Phys. Chem. Chem. Phys.* **2017**, *19*, 29780−29794.
(30) Abraham, M. J.; Murtola, T.; Schulz, R.; Páll, S.; Smith, J. C.; Hess, B.; Lindahl, E. GROMACS: High performance molecular simulations through multi-level parallelism from laptops to supercomputers. *SoftwareX* **2015**, *1−2*, 19−25.
(31) Gumbart, J. C.; Beeby, M.; Jensen, G. J.; Roux, B. *Escherichia coli* peptidoglycan structure and mechanics as predicted by atomic-scale simulations. *PLoS Comput. Biol.* **2014**, *10*, No. e1003475.
(32) Jo, S.; Kim, T.; Iyer, V. G.; Im, W. CHARMM-GUI: a web-based graphical user interface for CHARMM. *J. Comput. Chem.* **2008**, *29*, 1859−1865.
(33) Klauda, J. B.; Venable, R. M.; Freites, J. A.; O'Connor, J. W.; Tobias, D. J.; Mondragon-Ramirez, C.; Vorobyov, I.; MacKerell, A. D., Jr.; Pastor, R. W. Update of the CHARMM all-atom additive force field for lipids: validation on six lipid types. *J. Phys. Chem. B* **2010**, *114*, 7830−7843.
(34) Durell, S. R.; Brooks, B. R.; Ben-Naim, A. Solvent-induced forces between two hydrophilic groups. *J. Phys. Chem. A* **1994**, *98*, 2198−2202.
(35) Majhi, A. K.; Kanchi, S.; Venkataraman, V.; Ayappa, K.; Maiti, P. K. Estimation of activation energy for electroporation and pore growth rate in liquid crystalline and gel phases of lipid bilayers using molecular dynamics simulations. *Soft Matter* **2015**, *11*, 8632−8640.
(36) Vázquez-Laslop, N.; Lee, H.; Hu, R.; Neyfakh, A. A. Molecular sieve mechanism of selective release of cytoplasmic proteins by osmotically shocked *Escherichia coli*. *J. Bacteriol.* **2001**, *183*, 2399−2404.
(37) Demchick, P.; Koch, A. L. The permeability of the wall fabric of *Escherichia coli* and Bacillus subtilis. *J. Bacteriol.* **1996**, *178*, 768−773.
(38) Constantinides, P. P.; Steim, J. M. Physical properties of fatty acyl-CoA. Critical micelle concentrations and micellar size and shape. *J. Biol. Chem.* **1985**, *260*, 7573−7580.
(39) Malik, W. U.; Jain, A. Electrometric determination of critical micelle concentration of soap solutions. *J. Electroanal. Chem. Interfacial Electrochem.* **1967**, *14*, 37−41.
(40) Allen, W. J.; Lemkul, J. A.; Bevan, D. R. GridMAT-MD: a grid-based membrane analysis tool for use with molecular dynamics. *J. Comput. Chem.* **2009**, *30*, 1952−1958.
(41) Helfrich, W. Steric interaction of fluid membranes in multilayer systems. *Z. Naturforsch. A* **1978**, *33*, 305−315.
(42) Venable, R. M.; Brown, F. L.; Pastor, R. W. Mechanical properties of lipid bilayers from molecular dynamics simulation. *Chem. Phys. Lipids* **2015**, *192*, 60−74.
(43) Ziegler, M. J.; Vernier, P. T. Interface water dynamics and porating electric fields for phospholipid bilayers. *J. Phys. Chem. B* **2008**, *112*, 13588−13596.
(44) Gupta, R.; Rai, B. Electroporation of skin stratum corneum lipid bilayer and molecular mechanism of drug transport: A molecular dynamics study. *Langmuir* **2018**, *34*, 5860−5870.
(45) Reigada, R. Electroporation of heterogeneous lipid membranes. *Biochim. Biophys. Acta, Biomembr.* **2014**, *1838*, 814−821.
(46) Böckmann, R. A.; de Groot, B. L.; Kakorin, S.; Neumann, E.; Grubmüller, H. Kinetics, statistics, and energetics of lipid membrane electroporation studied by molecular dynamics simulations. *Biophys. J.* **2008**, *95*, 1837−1850.
(47) Churchward, C. P.; Alany, R. G.; Snyder, L. A. Alternative antimicrobials: the properties of fatty acids and monoglycerides. *Crit. Rev. Microbiol.* **2018**, *44*, 561−570.
(48) Campbell, A. N.; Lakshminarayanan, G. Conductances and surface tensions of aqueous solutions of sodium decanoate, sodium laurate, and sodium myristate, at 25 and 35. *Can. J. Chem.* **1965**, *43*, 1729−1737.
(49) Alinnor, I.; Enenebeaku, C. Adsorption Characteristics of Sodium Oleate onto Calcite. *Int. Res. J. Pure Appl. Chem.* **2014**, *4*, 88.
(50) Huang, K.-C.; Lin, C.-M.; Tsao, H.-K.; Sheng, Y.-J. The interactions between surfactants and vesicles: Dissipative particle dynamics. *J. Chem. Phys.* **2009**, *130*, No. 06B622.
(51) Santos, A. P.; Panagiotopoulos, A. Z. Determination of the critical micelle concentration in simulations of surfactant systems. *J. Chem. Phys.* **2016**, *144*, No. 044709.
(52) Debnath, A.; Thakkar, F. M.; Maiti, P. K.; Kumaran, V.; Ayappa, K. Laterally structured ripple and square phases with one and two dimensional thickness modulations in a model bilayer system. *Soft Matter* **2014**, *10*, 7630−7637.

(53) Liu, K.; Yang, L.; Peng, X.; Gong, H.; Wang, J.; Lu, J. R.; Xu, H. Effects of Conventional Surfactants on the Activity of Designed Antimicrobial Peptide. *Langmuir* **2020**, *36*, 3531−3539.
(54) Strahl, H.; Hamoen, L. W. Membrane potential is important for bacterial cell division. *Proc. Natl. Acad. Sci. U.S.A.* **2010**, *107*, 12281−12286.
(55) Jones, M. N.; Micelles, M.et al.*Micelles, monolayers, and biomembranes*; Wiley-Liss, 1995.
(56) Jackson, M. L.; Schmidt, C.; Lichtenberg, D.; Litman, B.; Albert, A. Solubilization of phosphatidylcholine bilayers by octyl glucoside. *Biochemistry* **1982**, *21*, 4576−4582.
(57) Kragh-Hansen, U.; le Maire, M.; Møller, J. V. The mechanism of detergent solubilization of liposomes and protein-containing membranes. *Biophys. J.* **1998**, *75*, 2932−2946.
(58) Wiener, M. C.; Horanyi, P. S. How hydrophobic molecules traverse the outer membranes of Gram-negative bacteria. *Proc. Natl. Acad. Sci. U.S.A.* **2011**, *108*, 10929−10930.

https://doi.org/10.1021/acs.langmuir.2c02520
Langmuir 2022, 38, 15714−15728